Ocean Surface Wave Measurement Using a Steerable High-Frequency Narrow-Beam Ground Wave Radar

E. W. GILL

Centre for Cold Ocean Resources Engineering, Memorial University, St. John's, Newfoundland, Canada

M. L. KHANDEKAR

Atmospheric Environment Service, Environment Canada, Downsview, Ontario, Canada

R. K. HOWELL

Department of Electrical Engineering, University of Victoria, Victoria, British Columbia, Canada

J. WALSH

Faculty of Engineering and Applied Science, Memorial University, St. John's, Newfoundland, Canada

(Manuscript received 15 November 1994, in final form 21 September 1995)

ABSTRACT

Ground wave radar is emerging as an important tool for routine monitoring of ocean surface conditions and for ship and sea-ice surveillance at ranges well beyond the line-of-sight horizon that limits conventional systems. A major Canadian advance in this field is the recent development of a long-range ground wave radar facility at Cape Race, Newfoundland. Owned and operated by the Northern Radar Systems Limited, this shore-based radar system can monitor ocean surface conditions over a 120° sector out to a range of 200 km for sea state and to a range of 300 km for ocean surface currents. The near-real-time surface wave parameters are extracted from the Doppler spectra of the frequency-modulated interrupted continuous wave ground wave radar system.

This paper presents a brief overview of the radar system and discusses the process of extracting the one-dimensional wave spectrum and significant wave height from the Doppler spectra. The latter involves both the direct inversion of the HF (high frequency) radar cross section of the ocean surface as well as the least square fitting of modeled HF spectra. The ground wave radar facility at Cape Race was used in the measurement of wave parameters during the SAR (synthetic aperture radar) wave spectra validation experiments, offshore Newfoundland during November 1991. The SAR is one of the sensors aboard the European Space Agency's Remote Sensing Satellite (*ERS-1*) launched in June 1991. The wave parameters deduced by the ground wave radar were evaluated against buoy measurements as well as against hindcast values from the operational wave model, Canadian Spectral Ocean Wave Model. The radar-deduced wave heights were also evaluated against wave height charts prepared routinely by the Meteorology and Oceanography Centre at Halifax, Nova Scotia. Overall, a very good agreement was obtained.

The utility of the radar for nearshore wave analysis and nowcasting, as well as for offshore surveillance, is discussed.

1. Introduction

Ground wave radar, as the name suggests, employs the ground wave mode of radio propagation where the radar signal is guided by the ocean surface to follow a path that essentially matches the earth's curvature. Consequently, ground wave signals may reach well beyond the normal line-of-sight horizon that limits the range of conventional radar systems. Ground wave radar operation in the high-frequency (HF) band (3–30 MHz) not only permits efficient ground wave propagation so that large detection ranges are obtained but also causes the signal to react strongly with the ocean surface. That the resulting HF backscatter contains a wealth of information relevant to ocean surface conditions has been verified extensively. Barrick (e.g., 1971, 1972, 1977) and, subsequently, Lipa and Barrick (e.g., 1982, 1986) pioneered efforts to derive ocean information from the HF spectra resulting from the signal–ocean surface interactions. Following their lead, Wyatt (1988, 1989) and more recently Howell and Walsh (1993a,b) have produced useful results. The work of Barrick and Lipa, to a large extent, also accounts for the well-established practice of using HF

Corresponding author address: Eric W. Gill, C-CORE, Memorial University of Newfoundland, St. John's, NF A1B 3X5, Canada.

© 1996 American Meteorological Society

ground wave radars to map ocean surface currents. While many advances have been made in the technological development of such radars, a continuing challenge for these systems is the measurement of ocean wave spectra and the estimation of ocean surface wind speed.

The recent construction of a long-range radar facility at Cape Race, Newfoundland, by Northern Radar Systems Limited (NRSL) represents an important advance in ground wave radar technology in Canada. Operating in the HF band, this shore-based system can monitor ocean surface conditions over a 120° sector out to a range of 200 km for sea state and to a range of 300 km for surface currents. In addition, the system can also track hard targets, such as ships and sea ice. The coverage area of the Cape Race radar out to its ship detection range of 200 km is shown in Fig. 1.

The purpose of this paper is to examine the ocean surface wave measuring capabilities of the Cape Race facility during its use in the validation of sea-state parameters associated with the European Space Agency's Remote Sensing Satellite (*ERS-1*) SAR (synthetic aperture radar) Wave Experiment (hereafter referred to as "the experiment") (Dobson et al. 1993). The algorithm used is a modification of that reported by Howell (1990). The radar-derived wave parameters—namely, significant wave height and the one-dimensional wave spectrum—are evaluated against buoy measurements as well as against the hindcast values generated by an operational wave model of the Atmospheric Environment Service (AES) called the Canadian Spectral Ocean Wave Model (CSOWM). The radar-measured wave heights are also compared against operational wave height charts prepared routinely by the Meteorology and Oceanography Centre (METOC) at Halifax, Nova Scotia. While the total experiment was conducted over a one-month period (November–December 1991), only five days were dedicated to wave measurement using the radar, the remaining time being devoted, almost exclusively, to surface current measurement (see Hickey et al. 1992). Nonetheless, the authors feel that the available results at least provide a preliminary indication of the feasibility of implementing the Cape Race radar for estimating sea-state parameters over a significant area of the nearshore region.

In section 2, the operational characteristics of the NRSL radar system are reviewed, and its use in the experiment is described. Section 3 briefly reviews the various backscatter mechanisms and presents Howell's algorithm and its modification necessitated by the frequency of operation of the radar. Section 4 contains a brief description of the operational wave model CSOWM, a basic version of which is currently run in operational mode at the Canadian Meteorological Centre (CMC) in Montreal, Quebec. In section 5, ocean surface wave parameters obtained by the radar system are compared with values obtained from other sources as referred to above. Finally, the utility of this radar system for wave analysis and surveillance is considered.

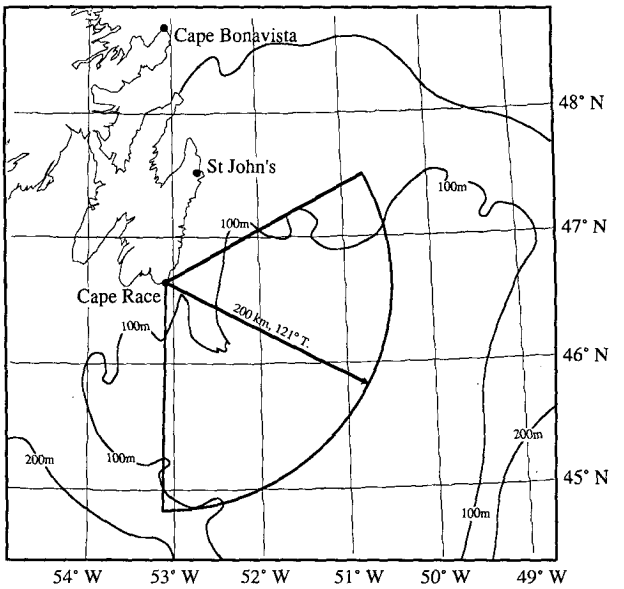

FIG. 1. Region of coverage for the ground wave radar system located at Cape Race, Newfoundland. The arrow represents the radar boresight.

2. The radar system

The NRSL facility, located on a 2.5-km strip of land at Cape Race, overlooks a large area of the Grand Banks region off the southeast shores of Newfoundland. The HF ground wave radar site consists of "receive" and "transmit" antennas, a receive–control–accommodations building, and a transmit building. The transmit antenna is a standard log-periodic dipole array. The ideal half-power beamwidth of this antenna is 120° (over perfect ground). The receive antenna, nearly a kilometer in length, is a 40-element linear array whose elements are planar diamond-shaped monopoles. The beamwidth increases from 2.5° broadside to 6° with 60° steering from broadside. The angular coverage is from a bearing of 61.0° to 181° (true) as measured from the site. The physical setup of the radar facility is shown schematically in Fig. 2.

The radar hardware system consists of analog receivers, a transmitter, a control section, and a digital processing section. The analog section provides basic discrimination and detection of the received radio signals and effects a digital conversion. In addition to providing detailed target detection and tracking, the output of the digital section is used in the analysis of oceanographic data, including currents and surface waves.

During low-interference periods, the radar range extends from 25 to about 200 km for wave measurements.

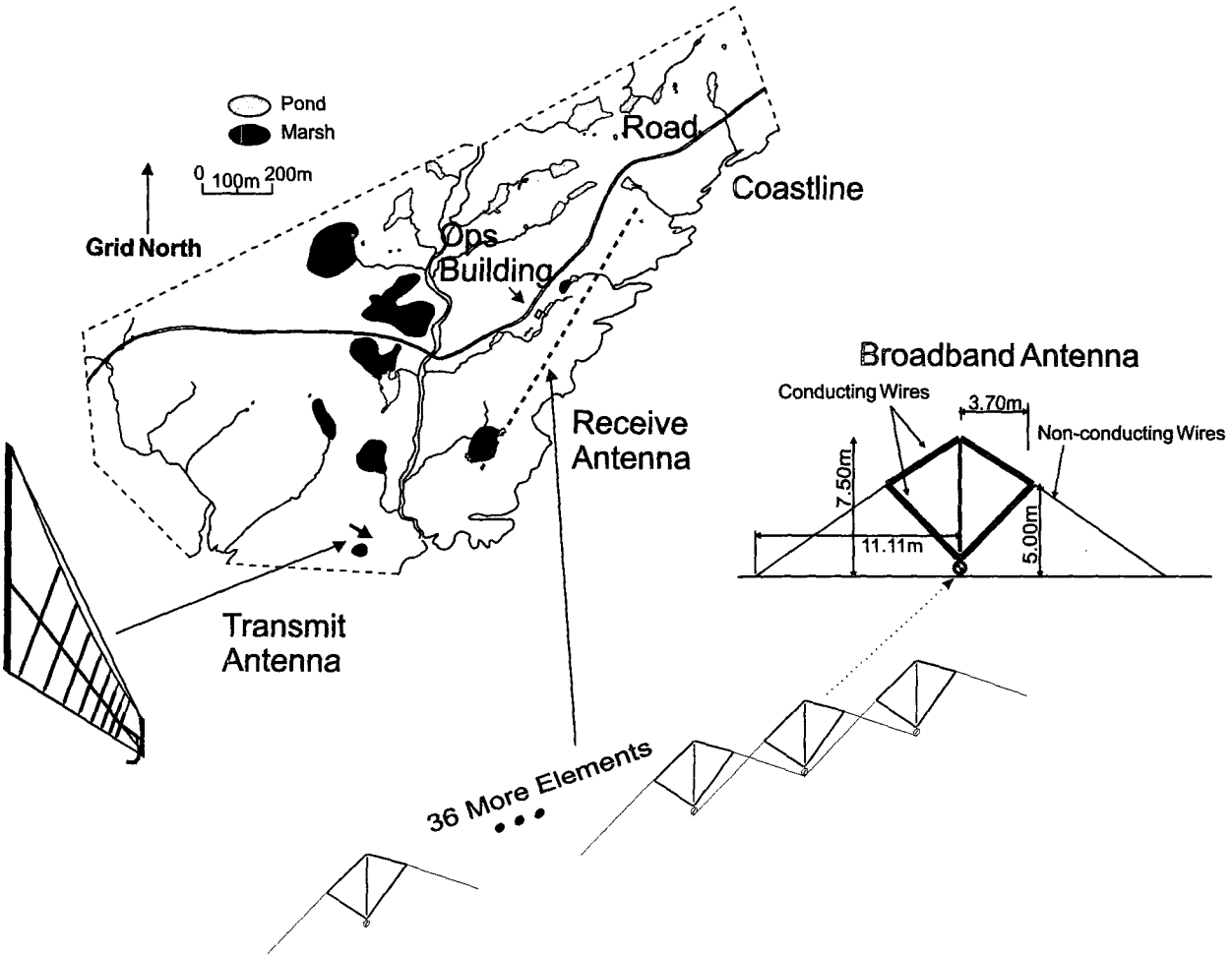

FIG. 2. A schematic showing the physical facilities of the Cape Race radar system and the environs. The receive antenna (RX) is 866 m long. The transmit antenna (TX) is a log-periodic array.

This range for sea-state measurements is a function of daily and seasonal variations of the ionosphere. As solar radiation becomes stronger, so does the capacity of the individual ionospheric layers to reflect high-frequency waves back to earth (Braun 1982). As a result, the system performance is usually enhanced at midday or during summer months, while it is somewhat diminished at night or during the winter months. This is a common characteristic of all HF radars.

For the duration of the experiment, the HF radar at Cape Race operated in a 375-kHz band with a center frequency of 6.75 MHz. The carrier signal was swept through this band with a period of 0.5 s and was gated on/off in a sequential periodic interruption. The radial resolution achieved by such a swept carrier signal is given by $c/2b$, where c is the HF propagation speed (approximately 3×10^8 m s^{-1} in free space) and b is the sweep bandwidth (375 kHz here); this gives a maximum radial resolution of about 400 m. The peak power of the system was 16 kW, the average being 2 kW. The sea state was monitored along eight different radar beam directions, and along each radar beam, measurements were analyzed in 25-km intervals. Over 40 000 km^2 of ocean area surrounding Cape Race (see Fig. 1) were monitored during the field experiment.

3. Wave measurement algorithm

a. HF backscatter from the ocean

Electromagnetic backscatter from the ocean surface has been a topic of investigation since the inception of radar. A typical Doppler spectrum of ocean backscatter recorded by the Cape Race radar system operating at 6.75 MHz is shown schematically in Fig. 3. The spectrum is generally characterized by two strong peaks appearing above and below the carrier frequency. The physical mechanism responsible for these "first order" peaks is coherent Bragg scatter. These Bragg peaks represent, for grazing incidence, radiation being reflected

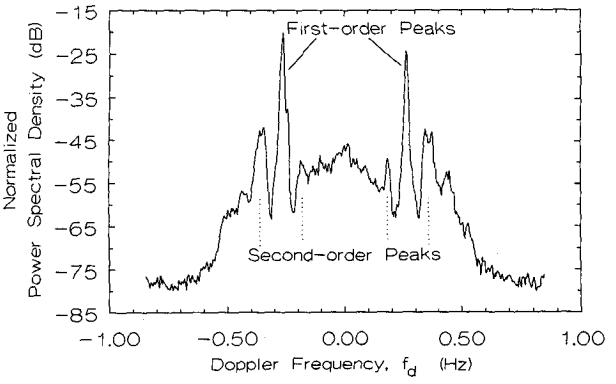

FIG. 3. An example of a Doppler spectrum observed by the HF radar system for an operating frequency of 6.75 MHz. Radial surface currents are determined from the positions of the first-order peaks, while the second-order peaks contain much of the ocean spectral information.

by ocean waves traveling toward or away from the radar and having a wavelength one-half that of the transmitted signal (Crombie 1955). The sidebands surrounding the Bragg peaks are due to nonlinear wave–wave interactions and higher-order Bragg scatter (Hasselmann 1971).

The radar spectrum of Fig. 3 is typical of those produced by the NRSL radar. For an operating frequency of 6.75 MHz, the prominent Bragg peaks ideally appear at the Doppler frequencies $f_B = \pm 0.265$ Hz according to the equation

$$f_B = \pm \frac{1}{\pi}\left(\frac{gk_0}{2}\right)^{1/2}, \quad (1)$$

where g is the gravitational acceleration and k_0 is the radar wavenumber. Underlying surface currents may cause these peaks to be shifted from their theoretical values, a fact that must be accounted for in the wave analysis.

The second-order scatter (see Barrick 1972; Walsh et al. 1990) is the dominant contributor to the continuum surrounding the first-order Bragg regions. Most of the second-order backscatter arises from the incident radiation reflecting from second-order ocean waves formed by the nonlinear wave–wave interaction between two first-order waves. In addition, a double scatter of the HF signal from two first-order ocean waves adds to this spectral energy. In both cases, backscatter will occur only if the ocean waves, with wave vectors $\mathbf{k}$ and $\mathbf{k}'$, respectively, satisfy the relation

$$\mathbf{k} + \mathbf{k}' = -2\mathbf{k}_0, \quad (2)$$

where the vector $\mathbf{k}_0$ lies in the look direction of the narrow radar beam.

Barrick (1972) was the first to derive the complete expressions for the second-order HF sea echo. More recently, Walsh et al. (1990) have developed similar models of the HF radar cross sections of the ocean surface to third order. Together, these theoretical results reveal that for a Doppler spectrum produced by radiation in the upper region of the HF band (between about 20 and 30 MHz) the second-order continuum adjacent to the Bragg peaks contains most of the ocean spectral information. However, the central transmit frequency of 6.75 MHz used in this experiment does not entirely conform to the criterion of "upper HF." In this case, a substantial amount of wave information may appear in ranges of the radar spectrum that are near-zero Doppler. The coupling of the transmitted radiation with the ocean surface is highly nonlinear for these near-zero Doppler portions of the spectrum, and the usual linearization schemes such as that presented by Barrick (1977), and implemented by others including Howell and Walsh (1993a), cannot be used alone to determine the major portion of the ocean spectral energy. This is done by means of fitting the experimental near-zero Doppler radar data to modeled data.

It should be noted also that the second-order portion of the Doppler spectrum may become saturated as the sea state intensifies (e.g., Barrick 1986). For an operating frequency of 6.75 MHz, this occurs when significant wave height exceeds 15 m. However, for the region of radar coverage here, wave climatology assessments (Wilson and Baird 1988) suggest that significant wave heights exceed 6 m only about 10% of the time in a given year, and a 15-m wave height is a once-in-20-year phenomenon. Thus, saturation was not a major issue for this experiment.

b. Estimation of the wave spectrum

The usual first step in any ocean surface parameter estimation algorithm involving HF radar is the normalization of the Doppler spectrum by dividing each half by the power contained in the local first-order peak (Barrick 1977). This is necessary in order to remove a variety of path/system gains and losses that scale the radar return. After normalization, the average second-order cross section of the scattering patch, given by Barrick as well as Walsh et al., takes the form

$$\sigma_2(\omega_d) = 2^5 k_0^4 \sum_{m,m'=\pm 1} \int_0^\infty \int_0^\pi \frac{|\Gamma|^2}{k'^4}[\mathbf{S}(k,\alpha) + \mathbf{S}(k,-\alpha)]\cdot\delta(\omega_d - m\omega_k - m'\omega_{k'})kdkd\theta, \quad (3)$$

where $\mathbf{S}$ is the ocean wave slope spectrum; $\alpha = \theta + (1 + m)\pi/2$, where θ is referenced to the radar look direction; δ is the Dirac delta function; ω_d is Doppler frequency (rad s^{-1}); and ω_k and $\omega_{k'}$ are the frequencies of the ocean waves responsible for the scattering. The quantity Γ is called the "coupling coefficient" and accounts for the hydrodynamic and electromagnetic effects associated with the scatter. Examination of the two cross-sectional models referred to above reveals that their difference lies primarily in the form of the

electromagnetic portion of Γ. The significance of this is discussed in more detail by Gill and Walsh (1992). Finally, m and m', which take values of ± 1, represent the four possible combinations of directions for the scattering wave vectors $\mathbf{k}$ and $\mathbf{k}'$.

Matrix representation of Eq. (3) by Howell (1990) essentially follows that of Lipa and Barrick (1982). To extract ocean wave spectra from the power spectra of a Doppler radar operating in the upper HF band, Howell "solved" the matrix equation by means of a singular value decomposition. Subsequently, Howell and Walsh (1993a) applied that scheme to an extensive quantity of experimental data. Howell's algorithm, as that of the previous investigators, can be used for Doppler frequencies f_d ($=\omega_d/2\pi$) in the intervals

$$0.64 f_B \leq |f_d| \leq 0.82 f_B$$

and

$$1.18 f_B \leq |f_d| \leq 1.36 f_B. \quad (4)$$

Outside these intervals, where the mapping of the ocean wave spectrum onto the radar spectrum is highly nonlinear, the inversion routine cannot be implemented. For the upper HF frequency range, this is not a difficulty since most of the ocean spectral energy will be extracted from the intervals indicated. The process can be accomplished in near-real time and has been tested for both narrow-beam as well as for omnidirectional arrays (Howell and Walsh 1993a,b). For a 25-MHz ground wave radar, nondirectional spectra and their associated parameters (e.g., significant wave height) can be obtained for ocean wave frequencies up to 0.25 Hz.

For the field experiment here, the radar operating frequency was 6.75 MHz, and the use of the Howell–Walsh algorithm yields the spectral energy density $E_R(f)$ of ocean waves ranging in frequency from about 0.0450 to 0.1262 Hz in increments of 0.00508 Hz. For ocean spectral energy that may lie in the frequency range from $f = 0.13$ to about $f = 0.3$ Hz, the Doppler interval given by the following expression is considered:

$$0.2 f_B \leq |f_d| \leq 0.6 f_B. \quad (5)$$

For the above frequency range, radar spectra are simulated from Eq. (3) by modeling the wave field as the product of a cardioid directional distribution (Longuet-Higgins et al. 1963) and a Pierson–Moskowitz spectrum (Pierson and Moskowitz 1964), which is commonly referred to as the PM spectrum and is defined by the following mathematical expression:

$$E_{\mathrm{PM}}(f) = \frac{0.0081}{(2\pi)^4 f^5} g^2 \exp\left[-1.25\left(\frac{f_p}{f}\right)^4\right], \quad (6)$$

where $f_p = 0.14 g/U_{19.5}$ is the frequency corresponding to the peak in the spectral energy of the PM spectrum and $U_{19.5}$ is the local wind speed (m s^{-1}) at the 19.5-m level above the ocean surface. It may be noted here that the relationship between the frequency spectrum and the nondirectional part of $\mathbf{S}(k, \alpha)$ of Eq. (3) can be easily determined from the dispersion relation for water waves [e.g., for deep water, this relation is simply $\omega = (gk)^{1/2}$, where ω is the angular frequency of the waves, k is their wavenumber, and g is the gravitational acceleration].

The use of the PM spectrum allows us to construct radar spectra for wind speeds ranging from 2 to 21 m s^{-1} at 1 m s^{-1} intervals. The 21 m s^{-1} upper limit on the wind speed reflects the fact that beyond this value the PM spectrum saturates for $f > 0.13$ Hz. The wind directions are incremented in 5° intervals. With these intervals of wind speed and wind direction a lookup table of simulated radar spectra is constructed. Next, using a technique similar to that successfully demonstrated for sky-wave radar by Maresca and Georges (1980), the measured ground wave radar data are least squares fitted to the simulated data for the region given by Eq. (5). The total estimate of the nondirectional wave spectrum $E(f)$ is then given by

$$E(f) = \begin{cases} E_R(f), & 0.0450\ \mathrm{Hz} \leq f \leq 0.1262\ \mathrm{Hz} \\ E_{\mathrm{PM}}(f), & 0.13\ \mathrm{Hz} \leq f \leq 0.30\ \mathrm{Hz}. \end{cases} \quad (7)$$

The significant wave height H_s can then be calculated according to the standard expression

$$H_s = 4[\textstyle\sum E(f)\Delta f]^{1/2}. \quad (8)$$

In Eq. (8), the summation extends from about 0.04 to about 0.30 Hz. This range is found to be quite adequate for most sea-state conditions within the radar coverage area. The nondirectional (one-dimensional) wave spectrum determined from Eq. (7) will be almost always unimodal in the wind-sea region from about 0.10 to 0.25 Hz.

4. The wave model CSOWM

The CSOWM is an operational spectral ocean wave model developed recently by the Meteorological Research Branch of the AES. The model has been designed to produce sea-state analysis and predictions over two separate oceanic regions, namely, the northwest Atlantic and the northeast Pacific. For each of these regions, the model operates over two separate grids covering a major portion of the North Atlantic and North Pacific Oceans. For each of these grids, a nested fine grid is designed that covers the nearshore regions of the Canadian Atlantic and the Canadian Pacific. The coarse and the nested fine grid of the northwest Atlantic are shown in Fig. 4. The coarse grid (with grid spacing of 1° latitude, which is about 110 km) has 2081 grid points, while the nested fine grid (with grid spacing one-third of the coarse grid spacing) has 2479 grid points covering the shelf region of the Canadian Atlantic. A similar nested grid (not shown) is designed to cover the Canadian Pacific region.

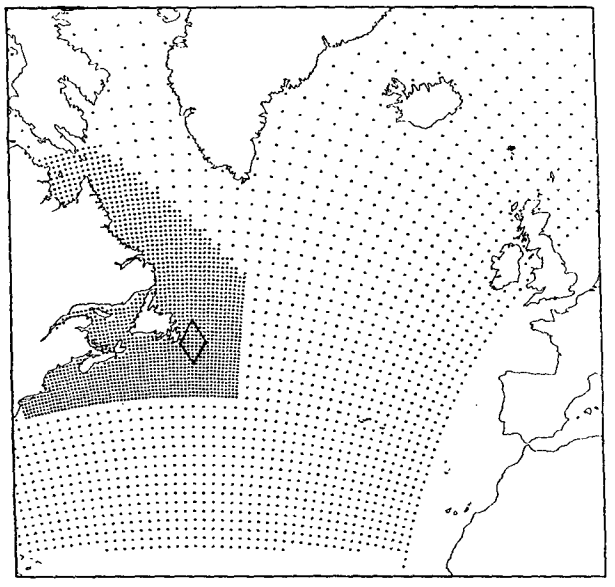

FIG. 4. The coarse and fine-grid mesh of CSOWM, covering a major portion of the northwest Atlantic. The coarse-grid spacing is about 110 km, while the fine-grid spacing is one-third of the coarse-grid spacing. The diamond-shaped area represents the crossover node for the descending and ascending passes of the satellite *ERS-1*.

The mathematical and physical framework of CSOWM is based on the wave model ODGP (Ocean Data Gathering Program) developed originally by Cardone et al. (1976). The energy balance equation, which is the basic equation for all spectral ocean wave models, is written in standard notation as

$$\frac{\partial E}{\partial t} + \nabla\cdot(\mathbf{C}_g E) = S. \qquad (9)$$

The various symbols in Eq. (9) are defined as follows:

- $E = E(f, \theta, \mathbf{x}, t)$ is the spectral energy density and is a function of frequency f, direction of wave propagation θ, position vector $\mathbf{x}$, and time t;
- $C_g = C_g(f, \theta)$ is the group velocity and is a function of frequency and direction in general—in deep water it is a function of frequency only; and
- $S = S(f, \theta, \mathbf{x}, t)$ is the net source function representing the physical processes that transfer energy to and from the wave spectrum—the source term S can be written symbolically as

$$S = S_{\text{in}} + S_{\text{nl}} + S_{\text{ds}}. \qquad (10)$$

In Eq. (10), S_{in} is the energy input to the wave field from the atmosphere, S_{nl} represents the transfer of energy associated with the nonlinear wave–wave interactions, and S_{ds} represents the energy dissipation, which includes dissipation in deep as well as shallow waters. Over the coarse grid of the CSOWM, only deep-water physics is employed, while over the fine-grid region of the model, shallow-water processes as represented by shoaling, refraction, bottom friction, and wavenumber scaling are included. For these shallow-water processes to be modeled, bathymetry is specified at all fine-grid locations. In the first-generation (1G) version of the model, the wind input term S_{in} and the dissipation term S_{ds} are included explicitly, while the nonlinear term S_{nl} is included only implicitly by modifying the atmospheric forcing term using the concept of a fully developed sea (e.g., Pierson 1982). In the third-generation (3G) version of CSOWM, all three source terms on the right side of Eq. (9) are explicitly included in the model calculations. The wind input term S_{in} is based on the field experimental study of Snyder et al. (1981), while the dissipation term S_{ds} is based on the whitecapping model of Hasselmann (1974) and its modification as proposed by Komen et al. (1984). The nonlinear wave–wave interaction term S_{nl} is explicitly calculated in the 3G version using the discrete interaction approximation, first proposed by Hasselmann and Hasselmann (1985) and applied here to the full two-dimensional spectrum of the CSOWM with 23 frequencies and 24 directions. More details of the model equations and their calculations can be seen in Khandekar et al. (1994).

The computer code of the CSOWM is designed with several optional packages, such as coarse only or coarse plus fine grid, deep only or deep plus shallow water physics, and a 1G or 3G algorithm for the source terms. It may be noted here that a basic version of the CSOWM—namely, coarse-grid, deep-water physics with a 1G algorithm—has been implemented in operation at the CMC in Montreal since January 1991. The model is run twice a day and is being driven by surface winds obtainable from the regional weather prediction model of the CMC. For the duration of the experiment, two versions of the model (1G and 3G) were run in a hindcast mode to generate wave model products. Also, two sets of wind fields, one identified as CMC winds and the other as MMM (man–machine mix) winds, were used to generate wave model products. Recent studies (e.g., Sanders 1990; Cardone 1992) on the structure of marine surface winds in extratropical storms have demonstrated the usefulness of a careful (and subjective) analysis of surface weather charts in generating accurate surface wind fields over an oceanic region. The impact of accurately determined ocean surface winds on wave model products has been demonstrated in studies by Khandekar (1989) and Khandekar and Eid (1987), among others. In view of these studies, wave model products using two sets of wind fields (CMC and MMM) were generated and evaluated against available buoy measurements for the duration of the experiment. Additional details on the CMC and MMM wind fields and on the impact of these wind fields on wave model products can be found in Khandekar et al. (1994). For the present study, we considered wave values generated by the 3G version of the CSOWM and (being) driven by both sets of wind

fields, namely, CMC and MMM. These wave values were evaluated against HF radar-generated values as well as against selected buoy data, as discussed in the following section. The shallow-water component of the model was not used here since the impact of bathymetry was considered minimal during the experiment.

5. Results and discussion

During the experiment, the HF radar collected nine 70-min sets of wave data from 11 November 1991 to 26 November 1991; these included four datasets collected during (local) night hours when the required 10-dB signal-to-noise ratio between the second-order return and the noise floor was not realized beyond about the 50-km range. Hence, our primary datasets for this study pertain to those that were collected during the (local) daytime hours. Each dataset consisted of eight radar beam directions along which measurements were analyzed at 25-km intervals extending from the radar site to about 200 km during low noise periods. Along each beam direction, the wave spectra were obtained by inverting the radar spectra averaged over 11 range cells, each cell having a radial width of 400 m. The radar spectrum for each cell was obtained using a 256-point fast Fourier transform (FFT). The azimuthal width of the ocean patch corresponding to each spectrum depends on range and bearing since, as noted earlier, the radar beamwidth varies with direction from a maximum of about 6° at 61° bearing to a minimum of about 3° at 121° bearing. Having obtained radar spectra at up to eight locations along each radar beam direction, the significant wave height was calculated according to Eq. (8). These radar-deduced wave parameters were evaluated against model-deduced and buoy-measured parameters at a total of five grid locations as shown in Fig. 5. Of these five locations, four were inside the diamond-shaped crossover node, and one was in the vicinity of buoy 44138, which was operated by the Marine Environmental Data Service, Ottawa, Ontario, as part of the Canadian network of buoys. The radar-deduced wave heights were also evaluated against wave height charts prepared and routinely issued by METOC. These evaluation results are discussed below.

Table 1 shows significant wave height values obtained from radar measurements compared against model-generated and buoy-measured values. The upper part of the table shows a comparison between radar and model wave heights, while the lower part compares radar-deduced values against available buoy measurements. As mentioned, model wave heights generated using two sets of wind fields are presented in Table 1 for comparison against radar-deduced values. The CMC winds were extracted from the operational weather prediction model of the CMC in Montreal, which uses an objective analysis procedure to generate surface level winds. The MMM winds were obtained through an analysis of surface weather charts, application of a marine planetary boundary layer model, and a subjective kinematic analysis over a limited domain of the CSOWM grid where additional ship and buoy wind data were available (see Khandekar et al. 1994). Thus, the wave heights generated by the model when driven by MMM winds are expected to be closer to the actual sea-state conditions that prevailed during the field experiment. An inspection of the wave height values in the upper half of the table reveals that in general the radar-deduced values compare quite favorably with both sets of model-generated values, with the MMM model showing a slight improvement over the CMC model. The lower half of the table compares radar values against buoy measurements, and once again the radar values show, in general, a very good agreement with available buoy measurements. It may be noted that the HF radar operations were restricted to short durations during the (local) morning and evening hours so as to approximately coincide with the ascending and descending passover times of the satellite, while the model and the buoy measurements were processed at fixed 3-h intervals. Consequently, the radar-deduced wave heights correspond to times that do not exactly coincide but are within 1 h of the times given in the table. Despite this time difference, the agreement between radar, model, and buoy values is very good.

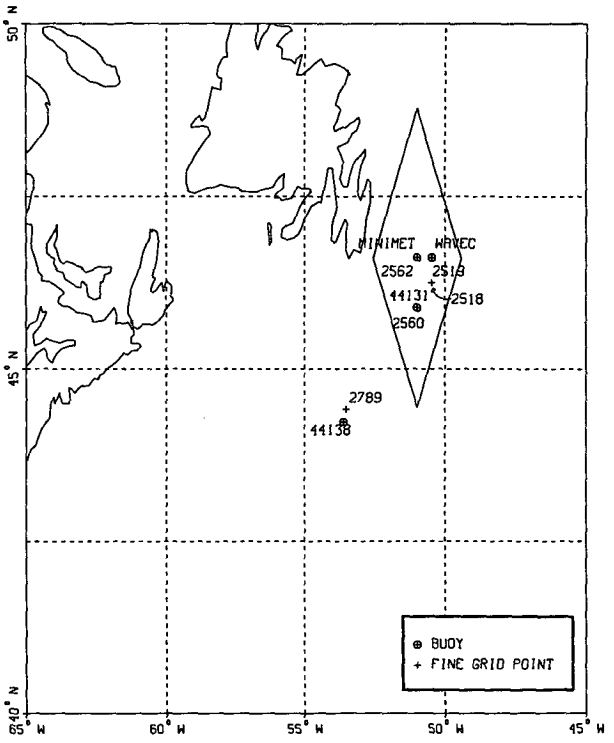

FIG. 5. Map showing gridpoint and buoy locations in the Canadian Atlantic where radar-deduced wave and wind parameters were evaluated. Inside the diamond-shaped crossover node, the buoy locations coincided exactly with the grid locations. The four-digit numbers refer to the fine-grid points of the wave model CSOWM.

TABLE 1. Comparisons between radar-deduced and model-generated as well as buoy-measured significant wave heights H_s at selected gridpoint locations. The model values are obtained using two sets of wind fields, namely, CMC and MMM.

Grid point	Measurement obtained by	H_s (m) at date and time (1991) 11 Nov 1500 UTC	14 Nov 1500 UTC	20 Nov 1500 UTC	21 Nov 0000 UTC	23 Nov 1500 UTC	26 Nov 0000 UTC
2518	Radar	1.4	3.2	2.2	2.7	2.4	3.7
	model CMC	0.8	2.5	2.4	2.8	2.6	3.1
	MMM	1.3	2.9	3.2	3.2	2.6	3.1
2519	Radar	0.8	3.1	3.1	3.0	3.8	3.8
	model CMC	0.8	2.6	2.4	2.8	2.4	3.8
	MMM	1.2	2.8	3.2	3.1	2.7	3.2
2560	Radar	1.2	2.3	3.0	2.8	2.6	3.6
	model CMC	0.8	2.6	2.3	2.7	2.2	3.7
	MMM	1.5	2.9	3.1	3.1	2.5	2.9
2562	Radar	0.8	2.4	3.1	2.7	2.7	3.8
	model CMC	0.7	2.9	2.4	2.7	2.3	3.9
	MMM	1.3	2.9	3.1	3.0	2.6	3.0
2789	Radar	1.2	3.5	3.0	N/A	3.2	4.2
	model CMC	1.4	2.0	2.0	2.3	1.5	3.5
	MMM	1.4	3.1	2.5	2.3	1.8	3.9
Mean bias	(Radar − CMC)	+0.2	+0.4	+0.6	+0.1	+1.0	+0.3
	(Radar − MMM)	−0.3	0	−0.1	−0.3	+0.8	+0.8
2519	Radar	0.8	3.1	3.1	3.0	3.8	3.8
	buoy (Wavec)	1.0	3.7	2.7	3.1	3.0	3.5
2560	Radar	1.2	2.3	3.0	2.8	2.6	3.6
	buoy (44131)	1.0	3.7	3.0	3.3	3.4	2.9
2789	Radar	1.2	3.5	3.0	N/A	3.2	4.2
	buoy (44138)	1.5	3.4	3.0	2.9	2.4	3.2
Mean bias	(Radar-buoy)	−0.1	−0.6	+0.1	−0.3	+0.8	+0.7

Next, an attempt was made to evaluate the radar-deduced values spatially by comparing them against the METOC wave height charts. Figure 6 shows METOC wave charts at two selected map times on which radar-deduced wave heights are plotted for three selected radar beam directions. Along each radar beam direction, wave height values are plotted at arbitrarily selected distances varying from 50 to 150 km. The METOC charts are drawn subjectively, taking into account available buoy and ship reports and applying the principle of continuity of wave fields (see Morgan 1971). The METOC wave chart provides a synoptic description of the wave field based on available data and is thus representative of "sea truth" over a given area. The wave height values deduced by the HF radar and plotted along the radar beam directions appear to be in very good agreement with the (background) wave field of the METOC charts as displayed in Fig. 6.

Two examples of validating radar-deduced one-dimensional (1D) spectra against buoy and model-generated spectra are presented in Fig. 7, which shows two sets of 1D spectra at two selected times. Also shown in Fig. 7 are values of significant wave heights corresponding to various spectra. The radar-deduced spectra as well as model-generated spectra are, in general, unimodal and smooth, whereas the buoy spectra typically exhibit multimodal structure with minor fluctuations associated with individual peaks. The radar-deduced spectrum for 20 November 1991 in Fig. 7 appears to be in excellent agreement with MMM model spectrum and in broad agreement with the buoy spectrum. The radar spectrum shows one sharp peak at about 0.14 Hz in agreement with the MMM model-generated peak and a secondary peak at about 0.08 Hz in accordance with the buoy spectrum. For 23 November 1991 the buoy spectrum in Fig. 7 has two sharp peaks: one located around 0.075 Hz, and the other at about 0.11 Hz. The radar spectrum does produce two peaks; however, the second peak at higher frequency is centered at around 0.15 Hz instead of at 0.11 Hz, where the peak of the buoy spectrum is located. The two model spectra (CMC and MMM) appear to be in good agreement with the main peak of the buoy spectrum. Once again, it must be noted that the buoy spectra refer to the Wavec buoy located at grid point 2519, which provided the nearest available buoy spectra for verification against radar and model spectra at grid point 2562 (see Fig. 5). Despite these spatial differences, the agreement between the radar and buoy spectra is quite encouraging.

6. Concluding remarks

The results presented in this study have helped us demonstrate the capabilities of the HF radar system lo-

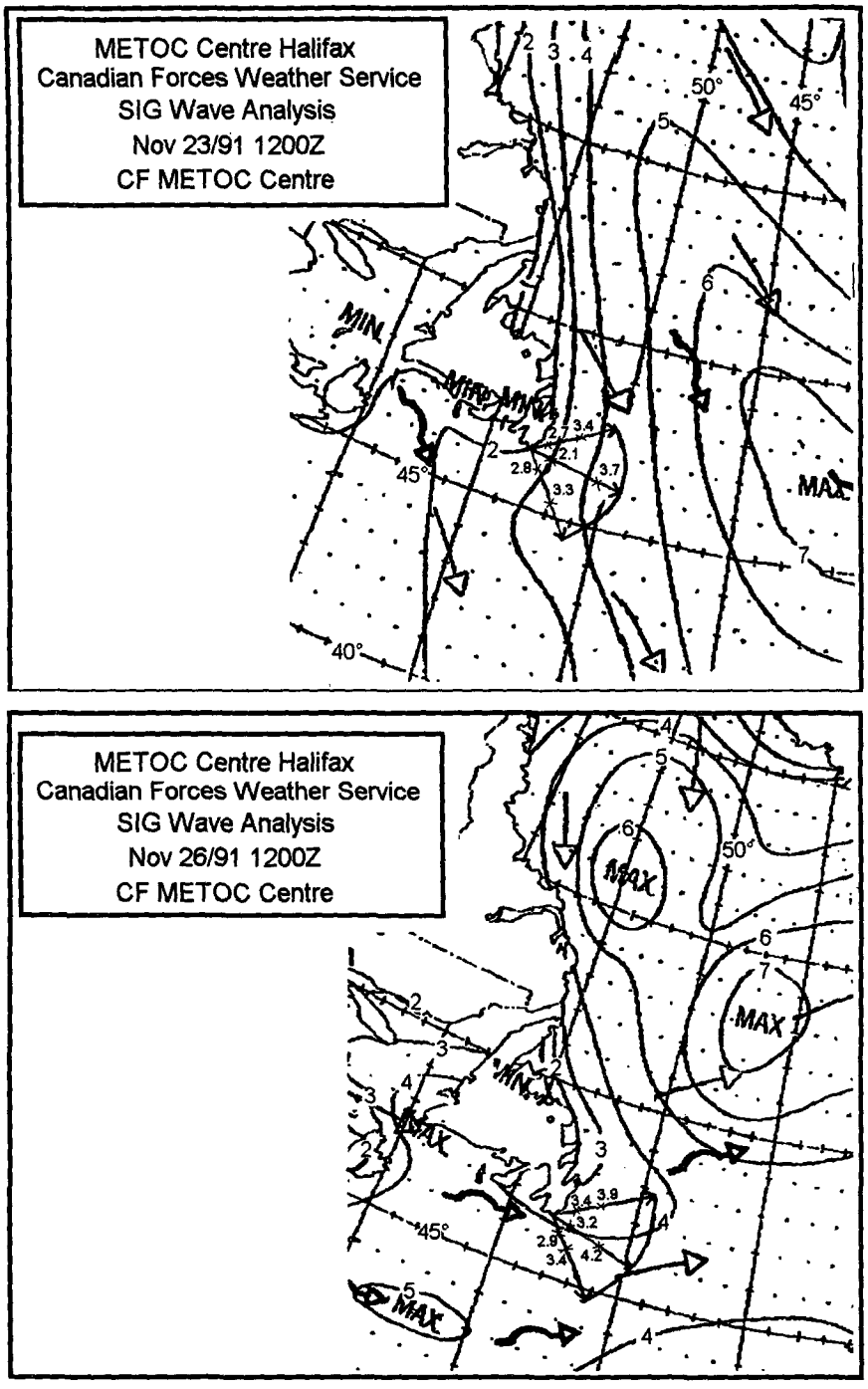

FIG. 6. Two examples of radar-deduced wave heights compared against the background of METOC wave height charts at two selected map times during the field experiment. Wave height values (m) deduced from radar measurements are plotted along three arbitrarily chosen radar beam directions with bearing of 62°, 100°, and 150°, respectively, from true north.

cated at Cape Race. An excellent overall agreement among the radar, model, and buoy values for significant wave heights in Table 1 and among the various 1D spectra of Fig. 7, has provided a high degree of confidence in the measurements of wave parameters by the Cape Race FMICW radar system. As described in section 3, the main wave products of this prototype radar are the one-dimensional wave energy spectrum and sig-

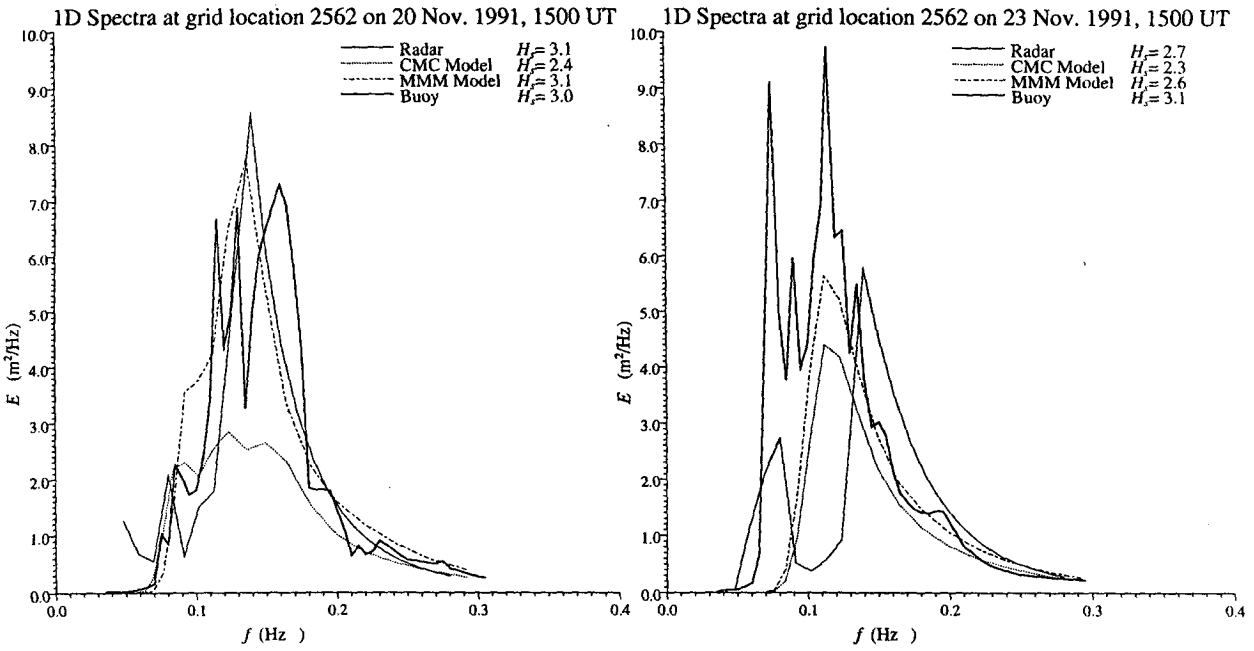

FIG. 7. Two examples of radar-deduced 1D wave spectra compared against model-generated and buoy-measured spectra. Also shown in the inset are values of significant wave height associated with these spectra.

nificant wave height. These parameters can be provided in near-real time out to a range of approximately 200 km from the shore. The range is expected to be enlarged in the near future following the upgrading of the Cape Race radar facilities.

The utility of the radar system is not limited to the measurement of ocean surface parameters. In addition to this important feature, the Cape Race radar can track ships, sea ice, and low-flying aircraft (Khan et al. 1993), features that will, among other applications, extend its usefulness to search and rescue operations. Such versatility makes this radar system a strategic tool for real-time monitoring of the Grand Banks region.

Acknowledgments. We would like to express our sincere thanks to the NRSL for providing their radar facility for the duration of the SAR wave spectra validation experiment. Thanks are also due to Ms. Ruth Tung of the AES for expertly typing the paper.

This study was primarily supported through the Government of Canada's Atlantic Fisheries Adjustment program (northern Cod Science Program) and in collaboration with Dr. Jim Helbig of the Department of Fisheries and Ocean Science at St. John's, Newfoundland. A secondary support came from the Panel on Energy Research and Development (PERD) of the Government of Canada.

REFERENCES

Barrick, D. E., 1971: Dependence of second-order Doppler sidebands in HF sea echo upon sea state. *IEEE G-AP Int. Symp. Digest,* 194–197.

——, 1972: Remote sensing of sea state by radar. *Remote Sensing of the Troposphere,* V. Derr, Ed., U.S. Government Printing Office, 1–46.

——, 1977: Extraction of wave parameters from measured HF radar sea-echo Doppler spectra. *Radio Sci.,* **12,** 415–424.

——, 1986: The role of the gravity-wave dispersion relation when interpreting HF radar measurements. *IEEE J. Oceanic Eng.,* **OE-11,** 286–292.

Braun, G., 1982: *Planning and Engineering of Short Wave Links.* Siemens Aktiengesellschaft, 328 pp.

Cardone, V., 1992: On the structure of marine wind field in extratropical storm. Preprints, *Third Int. Workshop on Wave Hindcasting and Forecasting.* Montreal, PQ, Canada, Environment Canada, 54–66.

——, W. J. Pierson, and E. G. Ward, 1976: Hindcasting the directional spectra of hurricane generated winds. *J. Pet. Technol.,* **28,** 385–394.

Crombie, D. D., 1955: Doppler spectrum of sea echo at 13.56 Mc./s. *Nature,* **175,** 681–682.

Dobson, F. W., S. D. Smith, R. J. Anderson, P. W. Vachon, D. Vandemark, J. R. Buckley, M. Allingham, M. Khandekar, R. Lalbeharry, and E. Gill, 1993: The Grand Banks ERS-1 SAR wave experiment. *Eos, Trans. Amer. Geophys. Union,* **74,** 41, 44–45.

Gill, E., and J. Walsh, 1992: Extraction of ocean wave parameters from HF backscatter received by a four-element array: Analysis and application. *IEEE J. Oceanic Eng.,* **17,** 376–386.

Hasselmann, K., 1971: Determination of ocean wave spectra from Doppler return from sea surface. *Nature, Phys. Sci.,* **229,** 16–17.

——, 1974: On the spectral dissipation of ocean waves due to white capping. *Bound.-Layer Meteor.,* **6,** 107–127.

Hasselmann, S., and K. Hasselmann, 1985: Computations and parameterization of the nonlinear energy transfer in a gravity-wave spectrum. Part I: New method for efficient computations of the exact nonlinear transfer integral. *J. Phys. Oceanogr.,* **15,** 1369–1377.

Hickey, K., E. W. Gill, J. Walsh, and B. Dawe, 1992: Results of the surface current and waves measurement program using the Northern Radar Cape Race Radar System. Rep. 92-C10, Centre for Cold Oceans Resources Eng., St. John's, NF, Canada, 269 pp.

Howell, R., 1990: An algorithm for extraction of ocean wave spectra from narrow beam HF radar backscatter. M.S. thesis, Faculty of Engineering and Applied Science, Memorial University of Newfoundland, 108 pp.

——, and J. Walsh, 1993a: Measurement of ocean wave spectra using a narrow beam HF radar. *IEEE J. Oceanic Eng.*, **18,** 296–305.

——, and ——, 1993b: Measurements of ocean wave spectra using a ship-mounted HF radar. *IEEE J. Oceanic Eng.*, **18,** 306–310.

Khan, R., E. W. Gill, S. A. Saoudy, K. Hickey, B. J. Dawe, and J. Walsh, 1993: An FMICW Radar. *Proc. IEEE Nat. Radar Conf.*, Boston, MA, IEEE, 107–112.

Khandekar, M. L., 1989: *Operational Analysis and Prediction of Ocean Wind Waves.* Coastal and Estuarine Studies, No. 33, Springer-Verlag, 214 pp.

——, and B. M. Eid, 1987: Wind specification for spectral ocean wave models. *Proc. 20th Coastal Eng. Conf.*, Taiwan, Amer. Soc. Civil Eng., 354–365.

——, R. Lalbeharry, and V. Cardone, 1994: The performance of the Canadian Spectral Ocean Wave Model (CSOWM) during the Grand Banks ERS-1 SAR wave spectra validation experiment. *Atmos.–Ocean,* **32,** 31–60.

Komen, G., S. Hasselmann, and K. Hasselmann, 1984: On the existance of a fully developed wind-sea spectrum. *J. Phys. Oceanogr.*, **14,** 1271–1285.

Lipa, B., and D. Barrick, 1982: Analysis methods for narrow-beam high-frequency radar sea echo. Tech. Rep. ERL 420-WPL 56, NOAA, Boulder, CO, 54 pp.

——, and ——, 1986: Extraction of sea state from HF radar sea echo: Mathematical theory and modeling. *Radio Sci.*, **21,** 81–100.

Longuet-Higgins, M., D. Cartwright, and N. Smith, 1963: Observations of the ocean wave spectrum of sea waves using the motions of a floating buoy. *Ocean Wave Spectra,* Prentice-Hall, 111–136.

Maresca, J. W., and T. M. Georges, 1980: Measuring rms wave height and the scalar ocean wave spectrum with HF skywave radar. *J. Geophys. Res.*, **85**(C5), 2759–2771.

Morgan, M. R., 1971: The analysis and forecasting of sea and swell conditions in deep water. Tech. Memo. TEC 763, Atmospheric Environment Service, Downsview, ON, Canada, 32 pp.

Pierson, W. J., 1982: The spectral ocean wave model (SOWM); A Northern Hemisphere computer model for specifying and forecasting ocean wave spectra. Final Rep. DINSRDC82/11, U.S. Naval Oceanography Command Detachment, Ashville, NC, 201 pp.

——, and L. Moskowitz, 1964: A proposed spectral form for fully developed seas based upon the similarity theory of S. A. Kitiagorodskii. *J. Geophys. Res.*, **69,** 5181–5190.

Sanders, F., 1990: Surface analysis over the oceans—Searching for sea truth. *Wea. Forecasting,* **5,** 596–612.

Snyder, R. L., F. W. Dobson, J. A. Elliott, and R. B. Long, 1981: Array measurements of atmospheric pressure fluctuations above surface gravity waves. *J. Fluid Mech.*, **102,** 1–59.

Walsh, J., R. Howell, and B. Dawe, 1990: Model development for evaluation studies of ground wave radar. Rep. 90-C14, Centre for Cold Oceans Resources Eng., St. John's, NF, Canada, 113 pp.

Wilson, J. R., and W. F. Baird, 1988: An assessment of the state of knowledge of east coast offshore wave climatology. Canadian Tech. Rep. of Hydrography and Ocean Sciences 63, 158 pp.

Wyatt, L. R., 1988: Significant waveheight measurement with HF radar. *Int. J. Remote Sens.*, **9,** 1087–1095.

——, 1989: Measuring the ocean wave directional spectrum with HF radar: The inversion problem. *Mathematics in Remote Sensing,* S. R. Brooks, Ed., Clarendon, 279–291.